Nano Energy 30 (2016) 517–522

Contents lists available at ScienceDirect

Nano Energy

journal homepage: www.elsevier.com/locate/nanoen

Mesoporous SnO_2 electron selective contact enables UV-stable perovskite solar cells

Bart Roose[a], Juan-Pablo Correa Baena[b], Karl C. Gödel[c], Michael Graetzel[d], Anders Hagfeldt[b], Ullrich Steiner[a], Antonio Abate[a,d,*]

[a] Adolphe Merkle Institute, Chemin des Verdiers 4, CH-1700 Fribourg, Switzerland
[b] Swiss Federal Institute of Technology (EPFL), Laboratory of Photomolecular Science, Station 6, CH-1015 Lausanne, Switzerland
[c] Cavendish Laboratory, Department of Physics, University of Cambridge, J J Thomson Avenue, Cambridge CB3 0HE, United Kingdom
[d] Swiss Federal Institute of Technology (EPFL), Laboratory of Photonics and Interfaces, Station 6, CH-1015 Lausanne, Switzerland

ARTICLE INFO

Keywords:
Perovskite solar cell
Hysteresis
Perovskite stability
SnO_2
UV stability

ABSTRACT

Perovskite solar cells are a promising new technology for large scale energy applications. The current major challenge for commercialization is increasing the device lifetime under real working conditions. State-of-the-art perovskite solar cells are prepared using TiO_2 as electron selective contact. In sealed devices, however, a reversible UV light activated performance degradation mechanism was observed. In this study, it is demonstrated that replacing TiO_2 with a SnO_2 electron selective contact enables stable perovskite solar cells working under UV light in an inert atmosphere. Contrary to previous reports on SnO_2 based perovskite solar cells, it is shown that a mesoporous electron selective contact is required to achieve UV stable perovskite solar cells.

1. Introduction

The power conversion efficiency (PCE) of perovskite solar cells (PSCs) has in recent years rapidly increased from 3.8% [1–3] to more than 22%, now rivaling the efficiency of market reference silicon solar cells [4]. Having passed this first hurdle, it is now becoming more important to increase the stability of PSCs to pass the industry standards, *i.e.* a PCE loss of less than 0.5% per year over a life span of 25 years [5]. More robust perovskites [6], metal contacts [7] and hole transporting materials [8] have been demonstrated to be quite effective to enhance the lifetime of PSCs, even though device stability is still far from industrial standards [8]. A major loss in PCE was found to be caused by a rapid degradation in the performance of TiO_2-based devices caused by the exposure to UV light [9], which is the most common device configuration in state-of-the-art PSCs. This performance degradation arises from the desorption of O_2^- that passivates deep electronic traps caused by oxygen vacancies in the TiO_2 lattice [8]. Although this effect can be significantly reduced by doping [10,11], attempts have been made to replace TiO_2 altogether [12,13]. One promising alternative inorganic material for electron selective layers (ESL) is SnO_2. Due to the wider band-gap, SnO_2 absorbs less UV light and is thus more robust than TiO_2 under sunlight [14]. In addition, the bulk electron mobility in SnO_2 is two orders of magnitude higher than that of TiO_2 [15], and electron injection from perovskite into SnO_2 has been shown to be more efficient than into TiO_2 [16]. SnO_2 has been successfully implemented on lab scale as ESL in low-temperature processed planar PCSs, yielding a stabilized PCE of more than 19.5% [16–19]. However, the rapid and poorly controlled perovskite crystallization makes it difficult to scale up planar PSCs for industrial application. A porous ESL can overcome this problem by changing the surface wettability [20] to achieve uniform perovskite coverage over large areas [21,22]. A porous ESL has also been shown to be beneficial for electron extraction [20]. It is thus of interest to develop a mesoporous SnO_2 (m-SnO_2) ESL for the industrial production of stable and efficient PSCs. So far, the highest reported PCE for solution processed, high temperature sintered m-SnO_2 based PSCs has only been 6.5% (not-stabilized) [23]. PSCs employing low temperature m-SnO_2 deposition, however, have reached a PCE of 12% (not-stabilized) [22]. The deposition of a thin conformal coating of TiO_2 onto high temperature sintered m-SnO_2 has been reported to increase the PCE to 11.9% (not-stabilized) [24]. The addition of TiO_2, however, defeats the purpose of using SnO_2 as a potentially more stable alternative.

In this study we show that m-SnO_2 PSCs are more stable than planar SnO_2 and m-TiO_2 PSCs during maximum power point tracking under continuous full sunlight illumination (no UV filtering) in an inert atmosphere. A significant hurdle, however, is the low open circuit

* Corresponding author at: Adolphe Merkle Institute, Chemin des Verdiers 4, CH-1700 Fribourg, Switzerland.
E-mail addresses: Juan.Correa@epfl.ch (J.-P.C. Baena), antonio.abate@unifr.ch (A. Abate).

http://dx.doi.org/10.1016/j.nanoen.2016.10.055
Received 19 August 2016; Received in revised form 19 October 2016; Accepted 27 October 2016
Available online 28 October 2016

voltage (V_{OC}) and fill factor (FF) of m-SnO_2 compared to planar SnO_2 and m-TiO_2 PSCs. We show that the origin of this behavior is the poor electron selectivity of m-SnO_2 as processed at high temperature atop of fluorine doped tin oxide (FTO) as transparent conductive oxide (TCO) electrode. We have investigated two possible causes; cracking of the ESL upon heating, or fluorine migration [25]. Our data suggests that, at high temperature, fluorine migrates from FTO into SnO_2, doping the ESL to an extent where charge selectivity is compromised and recombination is increased. To circumvent this problem we prepared m-SnO_2 PSCs using aluminum doped zinc oxide (AZO) as TCO. Moreover, AZO has good conductivity (sheet resistance $< 10/\square$) and is low-cost, composed of abundant materials, easy to etch and has a high transmittance in the near-IR region [26]. Using this alternative TCO, a strong increase in PCE and a remarkable stability of m-SnO_2 based PSCs were achieved.

2. Experimental

2.1. Material characterization

Scanning electron microscopy was carried out on a Tescan MIRA 3 LMH with a field emission source operated at an acceleration voltage of 10 kV. Pore size was calculated using ImageJ. X-ray diffraction was measured using a Rigaku Ultima IV with a Cu Kα source.

2.2. Cyclic voltammetry

Electrochemical experiments were carried out using a Metrohm PGSTAT302N Autolab. A Ag/AgCl reference electrode was used in an aqueous electrolyte solution containing 0.5 M KCl (0.5 M), $K_4Fe(CN)_6$ (0.5 mM) and $K_3Fe(CN)_6$ (0.5 mM) [24]. Cyclic voltammograms were collected at a scan rate of 50 mV/s.

2.3. Solar cell preparation

Fluorine doped tin oxide coated glass slides (Sigma-Aldrich, ~7/□) and aluminum doped zinc oxide coated glass slides (Zhuhai Kaivo Optoelectronic Technology Co., < 10/□) were cleaned by sonication in 2% Hellmanex soap solution for 15 min. After rinsing with deionized water and ethanol the substrates were again sonicated with isopropanol and rinsed with acetone. The substrates were treated with UV-ozone for 5 min and a 30 nm thick SnO_2 ESL was deposited by spray pyrolysis at 450 °C from a precursor solution of butyltin trichloride (250 mM) in anhydrous ethanol [14]. Mesostructured SnO_2 electrodes were synthesized using a structure directing block-copolymer [27]. A tin oxide precursor sol was prepared by dissolving poly(1,4-isoprene-*b*-ethylene oxide) (25 mg, Polymer Source, Mn: PIp(50000)-PEO(12000), M_w/M_n: 1.05) in tetrahydrofuran (1 ml), after which tin(IV) chloride pentahydrate was added (80 mg) and stirred for 30 min. The resulting solution was spin-coated (4000 rpm, 10 s) onto the substrate. The films were annealed on a programmable hotplate (2000 W, Harry Gestigkeit GmbH) using a 45 min ramp to 450 °C followed by a dwell time of 30 min to remove the block-copolymer template and crystallize SnO_2. Perovskite and HTM were deposited according to the literature [28,29]. Perovskite films were deposited from a precursor solution containing FAI (1 M), PbI_2 (1.1 M), MABr (0.2 M), $PbBr_2$ (0.2 M) and CsI (0.075 M) in anhydrous DMF:DMSO 4:1 (v:v). The perovskite solution was spin-coated in a two-step program at 1000 and 6000 rpm for 10 and 20 s respectively. During the second step, 100 μL of chlorobenzene was poured onto the spinning substrate 5 s prior the end of the program. The substrates were then annealed at 100 °C for 1 h in a nitrogen glove box. Subsequently, the substrates were cooled down for a few minutes and a spiroOMeTAD (Luminescence Technology) solution (70 mM in chlorobenzene) doped with bis(trifluoromethylsulfonyl)imide lithium salt (Li-TFSI, Aldrich), tris(2-(1H-pyrazol-1-yl)-4-*tert*-butylpyridine)-cobalt(III)tris(bis(tri uoromethylsulfonyl)imide) (FK209, Dyenamo) and 4-*tert*-butylpyridine (TBP, Aldrich) was spun at 4000 rpm for 20 s. The molar ratios of additives for spiroOMeTAD were: 0.5, 0.03 and 3.3 for Li-TFSI, FK209 and TBP, respectively. Finally, 60 nm of gold was thermally evaporated under high vacuum on top of the device. Dye sensitized solar cells were fabricated by employing Z907-dye as light absorber instead of perovskite [14].

2.4. Optoelectronic measurements

For photovoltaic measurements, a solar simulator from ABET Technologies (Model 11016 Sun 2000) with a xenon arc lamp was used and the solar cell response was recorded using a Metrohm PGSTAT302N Autolab. The intensity of the solar simulator was calibrated to 100 mW/cm^2 using a silicon reference cell from ReRa Solutions (KG5 filtered). *J-V*-curves were measured in reverse bias (from high to low voltages), at a scan rate of 10 mV/s. For dark currents a scan rate of 25 mV/s was used. The active area of the cells was 0.148 cm^2 and cells measured two days after their preparation. Maximum power point tracking was used to perform stability experiments in a nitrogen filled glovebox. The measurements were done on devices stored in dry ambient air for 1 month and were brought into the nitrogen atmosphere just before the start of the measurements. Intensity modulated photovoltage spectroscopy (IMVS) was performed according to the procedure described in literature, using a white light LED driver at different light intensities and a Metrohm PGSTAT302N Autolab [30].

3. Results and discussion

3.1. Characterization of compact SnO_2

3.1.1. Scanning electron microscopy

AZO (Fig. 1a) and FTO (Fig. 1b) electrodes were coated with a thin compact ESL of SnO_2 by spray pyrolysis at 450 °C. On AZO, the ESL, consisting of densely packed particles, is clearly visible and therefore it is likely that this layer grows heteroepitaxially (Fig. 1c). In contrast, the ESL appears to have grown epitaxially on FTO and no distinct layer can be distinguished (Fig. 1d).

3.1.2. Cyclic voltammetry

To test the surface coverage and rectifying behavior of the SnO_2 ESL, cyclic voltammetry was performed in an aqueous solution of $Fe(CN)_6^{3-/4-}$ for both FTO (Fig. 2a) and AZO (Fig. 2b) substrates, onto which a SnO_2 ESL was deposited by spray pyrolysis at 450 °C. SnO_2 behaves like an electrochemically silent dielectric material against the $Fe(CN)_6^{3-/4-}$ redox couple [31]. The charge-transfer reaction is therefore assumed to occur exclusively at the bare TCO surface. The effective TCO surface area in contact with the electrolyte can be determined by dividing the peak current of the ESL covered substrate by the peak current of the bare TCO substrate [31], yielding an effective uncovered FTO area of 60%. In contrast, the ESL covered AZO substrate exhibited an effective uncovered AZO area of < 1%.

The poor apparent effective coverage of the SnO_2 ESL on FTO may have two causes; (i) thermal stresses could cause cracks/pores upon cooling and/or heating, (ii) fluorine migration from FTO to the SnO_2 ESL, making the two layers electronically equivalent. The first option is highly unlikely since the FTO and SnO_2 lattice constants match, while the wurtzite/cassiterite interface of the AZO/SnO_2 junction has a much higher lattice mismatch, which should cause a much larger strain [32]. This implies that SnO_2 on AZO should be more prone to cracking than SnO_2 on FTO, in contrast to our observation. Indeed, SEM micrographs show a conformal SnO_2 ESL on FTO and no evidence of (Fig. 1). Fluorine migration in SnO_2 has however been previously shown, at annealing temperatures similar to this study [25,33] and would explain the observed effects, since fluorine migration renders SnO_2 electronically equivalent to FTO and thereby results in a loss in electron

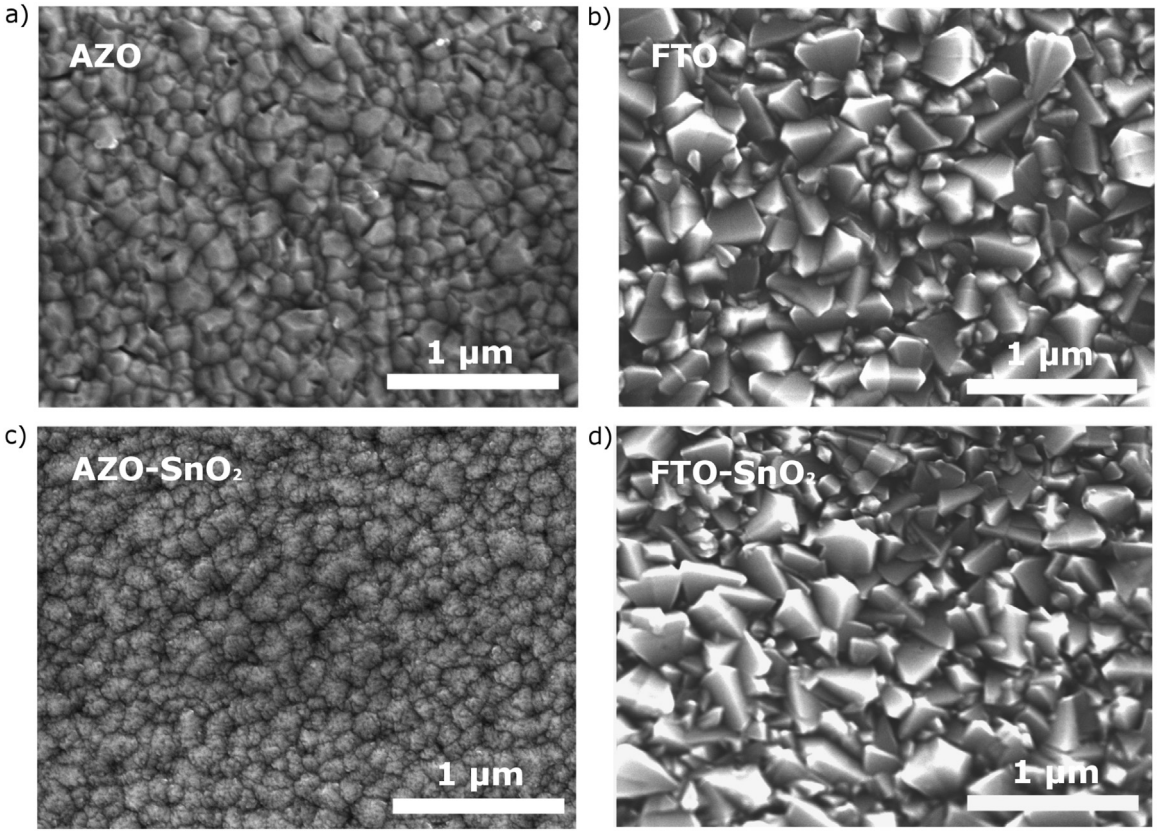

Fig. 1. SEM micrographs of (a) AZO, (b) FTO, (c) SnO_2 ESL on AZO and (d) SnO_2 ESL on FTO.

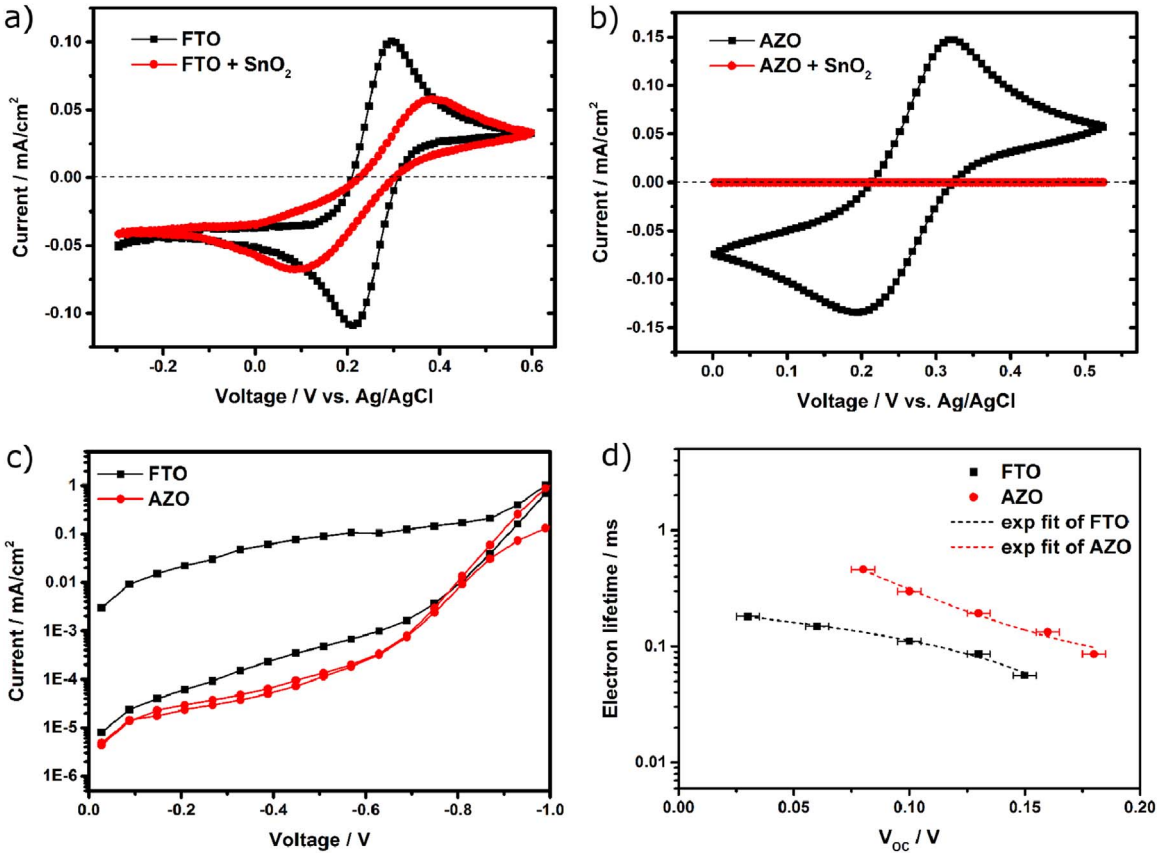

Fig. 2. Cyclic voltammograms of (a) a bare FTO electrode and FTO covered by a spray coated SnO_2 ESL, (b) a bare AZO electrode and AZO covered by a spray coated SnO_2 ESL. The scan rate was 50 mV/s and the electrolyte solution consisted of 0.5 mM $K_4Fe(CN)_6$ +0.5 mM $K_3Fe(CN)_6$ in 0.5 M aqueous KCl. (c) The minimal and maximal dark current of one batch (8 devices) of FTO and AZO based PSCs. (d) Electron lifetimes of DSSCs employing FTO and AZO as TCO as determined by IMVS.

selectivity.

3.1.3. Dark current-voltage scan

The poor electron selectivity of SnO_2 on FTO also becomes clear from the current-voltage scan under dark conditions of a complete PSC. The presence of a large dark current is an indication that the ESL is not effectively preventing the TCO from contacting the photoactive or hole transporting layers. Fig. 2c shows the minimal and maximal dark currents for a single batch of PSCs (8 devices). AZO based PSCs show a narrow dark-current distribution and overall low dark currents. On the other hand, FTO based PSCs exhibit a large variation in the dark current, with high overall values.

3.1.4. Intensity modulated photovoltage spectroscopy

The effect of the electron selectivity of SnO_2 coated TCO can be investigated by IMVS (Fig. 2d). Because of the overlap of the perovskite and metal oxide signals [11], dye sensitized solar cells (DSSCs) were used instead. From this measurement it becomes apparent that electron lifetimes are 2–3 times longer for DSSCs employing AZO as TCO, compared to DSSCs employing FTO as TCO, showing that recombination can be reduced by using AZO instead of FTO.

3.2. Characterization of m-SnO_2

m-SnO_2 electrodes were synthesized *via* block-copolymer assisted self-assembly [27]. The resulting films show a homogeneous coverage of the mesoporous material with a pore size of approximately 60 nm (Fig. 3a). X-ray diffraction (XRD) showed the formation of rutile SnO_2 (Fig. 3b). The average particle size was 10.9 ± 1.0 nm, calculated using the Scherrer equation [34].

3.3. Photovoltaic performance

The SEM micrograph in Fig. 4a shows the cross section of a photovoltaic device employing a ~100 nm thick layer of mesoporous SnO_2. A top-view SEM micrograph of the perovskite film is shown in S1. The photocurrent-voltage (*J-V*) curves of the PSCs measured under AM1.5 simulated solar light (100 mW/cm^2) illumination are shown in Fig. 4b. The photovoltaic parameters extracted from the *J-V*-curves; the open-circuit potential (V_{oc}), short-circuit current (J_{sc}), fill factor (FF), power conversion efficiency of the backward scan (PCE BW), power conversion of the forward scan (PCE FW) and the stabilized power output efficiency after 300 s are shown in Table 1. Incident photon conversion efficiency (IPCE) spectra are shown in S2, J_{sc} values are in agreement with those extracted from *J-V* curves. Since the PCE of PSCs is dependent on the way the device is measured (light and bias preconditioning, voltage scan speed and direction), additional measurements are required to verify the obtained PCE for device operation under realistic conditions [35]. By performing maximum power point tracking, a PCE value can be determined that accurately represents the efficiency of a device under real-world conditions. Device parameters clearly show a superior performance for AZO based devices owing to higher V_{oc} and FF, resulting in an increase in stabilized PCE from 8.7% for FTO to 11.6% for AZO based PSCs (averages of 8 devices). An increase in V_{OC} and FF is indicative of improved electron selectivity and reduced recombination at the ESL/perovskite interface, as was shown by IMVS measurements. Therefore, by replacing FTO with AZO it is possible to achieve an effective m-SnO_2 ESL.

3.4. Stability of PSCs

Planar SnO_2 and m-TiO_2 electrodes were prepared as previously reported [16], m-SnO_2 electrodes were prepared as described above. PSCs prepared with these electrodes were exposed to AM1.5 simulated solar light (100 mW/cm^2) illumination while tracking the maximum power point for 10 h in a nitrogen atmosphere. UV-induced degradation is a rapid degradation process, manifesting itself in the first 1–2 h of operation [9–11], so any UV-induced degradation should be evident in the 10 h testing period. To exclude an effect from the TCO, all device configurations were fabricated using FTO. The result of this maximum power point tracking is shown in Fig. 5. Initial power output (t=0), maximum power output (max) and final power output (t=10 h) are shown in Table 2, as well as the final power output divided by the maximum power output. The SnO_2-based devices show a remarkable increase over the first 1–2 h. Previous work has shown that this can be attributed to improved electron injection from the absorber into SnO_2, by an increase in the relative density of acceptor states as a result of a conduction band shift, induced by charging of the SnO_2 and a rearrangement of charge species at the absorber-SnO_2 interface [25,36]. On the other hand, m-TiO_2 shows a rapid decay during the first hour. It is known that defects in TiO_2 can be passivated by the adsorption of atmospheric oxygen. Under the influence of UV-light oxygen desorbs, leading to a rapid decrease in performance in oxygen free conditions [11], as is observed here. Fig. 5 shows that this is not the case for SnO_2-based PSCs, presumably because of the wider bandgap of SnO_2 compared to TiO_2. Another observation is that the mesoporous device power output reaches a plateau after these initial rapid changes, whereas the planar SnO_2 keeps steadily decreasing. The mesoporous network has been reported to inhibit the degradation or phase segregation of the perovskite by providing mechanical and chemical stability, inhibiting the penetration of harmful substances such as moisture, oxygen [22], or gold [7] into the perovskite layer. To rule out the possibility of a bad electron selective contact causing the decrease in performance of the planar SnO_2 PSCs it was verified that *J-*

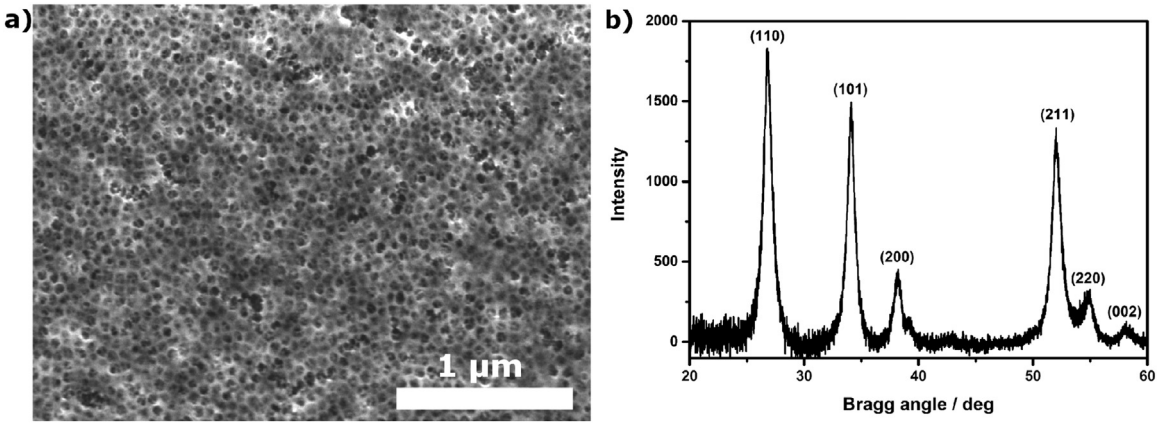

Fig. 3. (a) SEM micrograph of a mesoporous SnO_2 electrode synthesized by a solution deposition process in which pore formation was controlled by the self-assembly of a block-copolymer. (b) X-ray diffraction spectrum of the mesoporous SnO_2. All peaks can be assigned to rutile SnO_2 (indexed).

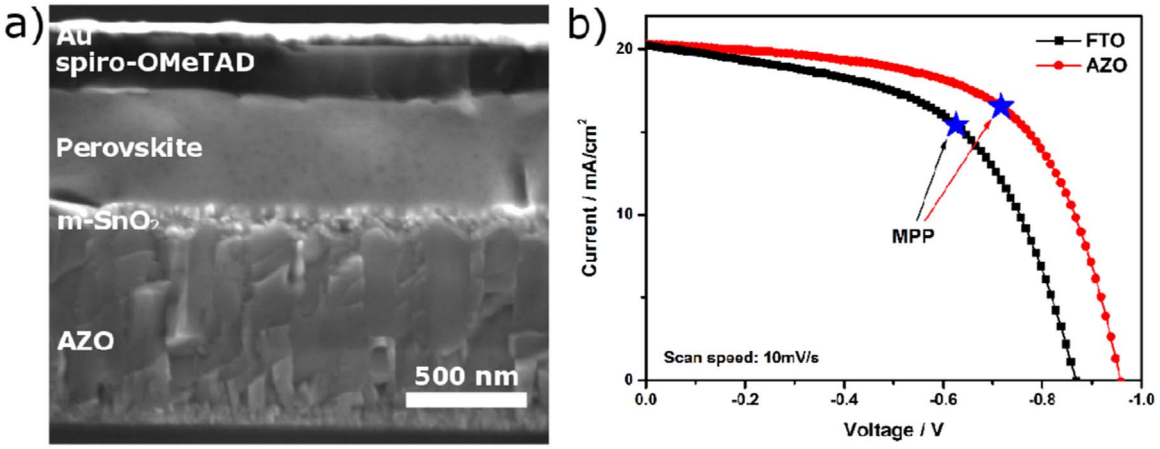

Fig. 4. (a) SEM cross-section of a photovoltaic device; AZO transparent conductive electrode, compact SnO_2 ESL, 100 nm mesoporous SnO_2, perovskite capping layer, spiroOMeTAD hole conducting layer and gold back contact. (b) *J-V* curves for PSCs employing FTO and AZO as transparent conducting electrodes. The *J-V*-curves were measured from forward bias to short circuit condition at a scan rate of 10 mV/s under AM1.5 simulated solar light (100 mW/cm^2) illumination. The cells were masked (0.148 cm^2) and characterized four days after their preparation. Table 1 lists the photovoltaic parameters for the two curves.

Table 1
Photovoltaic parameters of m-SnO_2 PSCs: open-circuit voltage (V_{oc}), short circuit current (J_{sc}), fill factor (FF), power conversion efficiency (PCE) extracted from the *J-V* curves and stabilized power conversion efficiency (Stab. PCE) after 300 s of maximum power point tracking. All values are averages for 8 devices. *J-V* characteristics were recorded sweeping the voltage from forward bias to short circuit condition at a scan rate of 10 mV/s. Active area: 0.148 cm^2.

TCO	V_{oc} [mV]	J_{sc} [mA/cm^2]	FF [%]	PCE BW [%]	PCE FW [%]	Stab. PCE (after300s) [%]
FTO average	887 ± 36	19.4 ± 0.9	56 ± 2	9.5 ± 0.8	8.2 ± 0.9	8.7 ± 1.0
FTO best	945	20.9	58	11.4	10.0	9.9
AZO average	965 ± 16	20.2 ± 1.4	60 ± 2	11.6 ± 1.3	10.3 ± 0.7	11.6 ± 0.7
AZO best	983	21.1	63	13.1	11.6	12.5

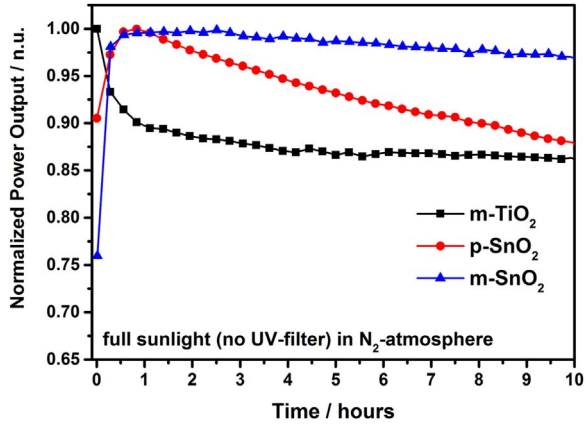

Fig. 5. Maximum power output normalized to the maximum value for m-SnO_2, m-TiO_2 and planar SnO_2 employing PSCs exposed to AM1.5 simulated solar light (100 mW/cm^2) illumination.

Table 2
Maximum power output of m-TiO_2, planar SnO_2 and m-SnO_2 PSCs at the start of the measurement (t=0), at the maximum (max) and at the end of the measurement (t=10 h).

	PCE, t=0	PCE, max	PCE, t=10 h
m-TiO_2	15.2	15.2	13.0
Planar SnO_2	16.1	17.9	15.6
m-SnO_2	7.3	10.7	10.4

V curves collected in the dark before and after the stability test were unchanged (S3). Overall, Fig. 5 shows superior stability for m-SnO_2 under these conditions, combining the UV-stability of SnO_2 with the mechanical and chemical stability of a mesoporous scaffold. This proves the importance of developing efficient m-SnO_2 based PSCs.

4. Conclusion

Highly efficient m-SnO_2-based PSCs are important because of their increased stability compared to m-TiO_2 and planar SnO_2 PSCs. Using FTO covered by SnO_2 is however problematic because of the migration of fluorine into the SnO_2, severely decreasing the electron selectivity of the ESL, as evidenced by cyclic voltammetry and dark current leakage. AZO is a viable alternative. Reduced recombination resulted in higher V_{OC} and FF values, leading to an increase in stabilized PCE from 8.7% to 11.6% (champion 13.1%), an increase of ~25%. This is an important step towards UV-stable PSCs.

Acknowledgements

This work was supported by the Swiss National Science Foundation [Program NRP70 No. 153990] and the Adolphe Merkle Foundation.

Appendix A. Supplementary material

Supplementary data associated with this article can be found in the online version at doi:10.1016/j.nanoen.2016.10.055.

References

[1] A. Kojima, K. Teshima, Y. Shirai, T. Miyasaka, J. Am. Chem. Soc. 131 (2009) 6050–6051.
[2] M.M. Lee, J. Teuscher, T. Miyasaka, T.N. Murakami, H.J. Snaith, Science 338 (2012) 643–647.
[3] H.-S. Kim, C.-R. Lee, J.-H. Im, K.-B. Lee, T. Moehl, A. Marchioro, S.-J. Min, R. Humphry-Baker, J.-H. Yum, J.E. Moser, M. Grätzel, N.-G. Park, Sci. Rep. 2 (2012) 591.
[4] National Renewable Energy Laboratory, Solar Cell Efficiency Chart. ⟨http://www.nrel.gov/ncpv/images/efficiency_chart.jpg⟩ (accessed July 2016).
[5] M.A. Maehlum, Lifespan of Solar Cells. ⟨http://energyinformative.org/lifespan-solar-panels/⟩ (accessed July 2016).
[6] J.-W. Lee, D.-H. Kim, H.-S. Kim, S.-W. Seo, S.M. Cho, N.-G. Park, Adv. Energy Mater. 5 (2015) 1501310.

[7] K. Domanski, J.-P. Correa-Baena, N. Mine, M.K. Nazeeruddin, A. Abate, M. Saliba, W. Tress, A. Hagfeldt, M. Graetzel, ACS Nano 10 (2016) 6306–6314.
[8] A. Abate, S. Paek, F. Giordano, J.P. Correa Baena, M. Saliba, P. Gao, T. Matsui, J. Ko, S.M. Zakeeruddin, K.H. Dahmen, A. Hagfeldt, M. Graetzel, M.K. Nazeeruddin, Energy Environ. Sci. 8 (2015) 2946–2953.
[9] T. Leijtens, G.E. Eperon, S. Pathak, A. Abate, M.M. Lee, H.J. Snaith, Nat. Commun. 4 (2013) 2885.
[10] S.K. Pathak, A. Abate, P. Ruckdeschel, B. Roose, K.C. Gödel, Y. Vaynzof, A. Sadhanala, S.-I. Watanabe, D.J. Hollman, N. Noel, A. Sepe, U. Wiesner, R. Friend, H.J. Snaith, U. Steiner, Adv. Funct. Mater. 24 (2014) 6046–6055.
[11] B. Roose, K.C. Gödel, S. Pathak, A. Sadhanala, J.P.C. Baena, B.D. Wilts, H.J. Snaith, U. Wiesner, M. Graetzel, U. Steiner, A. Abate, Adv. Energy Mater. 6 (2016) 1501868.
[12] J. You, L. Meng, T.-B. Song, T.-F. Guo, Y. Yang, W.-H. Chang, Z. Hong, H. Chen, H. Zhou, Q. Chen, Y. Liu, N. De Marco, Y. Yang, Nat. Nanotechnol. 11 (2016) 75–81.
[13] W. Chen, Y. Wu, Y. Yue, J. Liu, W. Zhang, X. Yang, H. Chen, E. Bi, I. Ashraful, M. Graetzel, L. Han, Science 350 (2015) 944948.
[14] P. Tiwana, P. Docampo, M.B. Johnston, H.J. Snaith, L.M. Herz, ACS Nano 5 (2011) 5158–5166.
[15] Q. Wali, A. Fakharuddin, R. Jose, J. Power Sources 293 (2015) 1039–1052.
[16] J.-P. Correa Baena, L. Steier, W. Tress, M. Saliba, S. Neutzner, T. Matsui, F. Giordano, T.J. Jacobsson, A.R.S. Kandada, S.M. Zakeeruddin, A. Petrozza, A. Abate, M.K. Nazeeruddin, M. Graetzel, A. Hagfeldt, Energy Environ. Sci. 8 (2015) 2928–2934.
[17] Z. Zhu, Y. Bai, X. Liu, C.-C. Chueh, S. Yang, A.K.-Y. Jen, Adv. Mater. 28 (2016) 6478–6484 1600619.
[18] J.Y. Seo, T. Matsui, J. Luo, J.-P. Correa-Baena, F. Giordano, M. Saliba, K. Schenk, A. Ummadisingu, K. Domanski, M. Hadadian, A. Hagfeldt, S.M. Zakeeruddin, U. Steiner, M. Graetzel, A. Abate, Adv. Energy Mater. 1600767 (2016).
[19] L. Xu, J. He, ACS Appl. Mater. Interfaces 4 (2012) 3293–3299.
[20] X. Bao, Y. Wang, Q. Zhu, N. Wang, D. Zhu, J. Wang, A. Yang, R. Yang, J. Power Sources 297 (2015) 53–58.
[21] Q. Liu, M.-C. Qin, W.-J. Ke, X.-L. Zheng, Z. Chen, P.-L. Qin, L.-B. Xiong, H.-W. Lei, J.-W. Wan, J. Wen, G. Yang, J.-J. Ma, Z.-Y. Zhang, G.-J. Fang, Adv. Funct. Mater. 1600910 (2016).
[22] E. Edri, S. Kirmayer, A. Henning, S. Mukhopadhyay, K. Gartsman, Y. Rosenwaks, G. Hodes, D. Cahen, Nano Lett. 14 (2014) 1000–1004.
[23] Y. Li, J. Zhu, Y. Huang, F. Liu, M. Lv, S. Chen, L. Hu, J. Tang, J. Yao, S. Dai, RSC Adv. 5 (2015) 28424–28429.
[24] G.S. Han, H.S. Chung, D.H. Kim, B.J. Kim, J.-W. Lee, N.-G. Park, I.S. Cho, J.-K. Lee, S. Lee, H.S. Jun, Nanoscale 7 (2015) 15284–15290.
[25] F.E. Akkad, S. Joseph, J. Appl. Phys. 112 (2012) 023501.
[26] X. Zhao, H. Shen, Y. Zhang, X. Li, X. Zhao, M. Tai, J. Li, J. Li, X. Li, H. Lin, ACS Appl. Mater. Interfaces 8 (2016) 7826–7833.
[27] S. Guldin, P. Docampo, M. Stefik, G. Kamita, U. Wiesner, H.J. Snaith, U. Steiner, Small 8 (2012) 432440.
[28] M. Saliba, T. Matsui, J.-Y. Seo, K. Domanski, J.-P. Correa-Baena, M.K. Nazeeruddin, S.M. Zakeeruddin, W. Tress, A. Abate, A. Hagfeldt, M. Graetzel, Energy Environ. Sci. 9 (2016) 1989–1997.
[29] A. Abate, D.R. Staff, D.J. Hollman, H.J. Snaith, A.B. Walker, Phys. Chem. Chem. Phys. 16 (2014) 1132–1138.
[30] P.R.F. Barnes, K. Miettunen, X. Li, A.Y. Anderson, T. Bessho, M. Grätzel, B.C. O'Regan, Adv. Mater. 25 (2013) 1881–1922.
[31] L. Kavan, N. Tétreault, T. Moehl, M. Grätzel, J. Phys. Chem. C 118 (2014) 16408–16418.
[32] D. Sidoti, S. Xhurxhi, T. Kujofsa, S. Cheruku, J.P. Correa, B. Bertoli, P.B. Rago, E.N. Suarez, F.C. Jain, J.E. Ayers, J. Appl. Phys. 109 (2011) 023510.
[33] J.-P. Correa-Baena, D.A. Kriz, M. Giotto, S.L. Suib, A.G. Agrios, RSC Adv. 6 (2016) 21326–21331.
[34] B. Roose, S. Pathak, U. Steiner, Chem. Soc. Rev. 44 (2015) 8326–8349.
[35] H.J. Snaith, A. Abate, J.M. Ball, G.E. Eperon, T. Leijtens, N.K. Noel, S.D. Stranks, J.T.-W. Wang, K. Wojciechowski, J. Phys. Chem. Lett. 5 (2014) 1511–1515.
[36] P. Tiwana, P. Docampo, M.B. Johnston, L.M. Herz, H.J. Snaith, Energy Environ. Sci. 5 (2012) 9566–9573.